Author's Accepted Manuscript

CHEMICAL ENGINEERING SCIENCE

Determination of the mixing time in a discontinuous powder mixer by using image analysis

B. Daumann, A. Fath, H. Anlauf, H. Nirschl

www.elsevier.com/locate/ces

Cite this article as: B. Daumann, A. Fath, H. Anlauf and H. Nirschl, Determination of the mixing time in a discontinuous powder mixer by using image analysis, *Chemical Engineering Science* (2009), doi:10.1016/j.ces.2009.01.032

Determination of the Mixing Time in a Discontinuous Powder Mixer by using image analysis

B. Daumann, A. Fath, ,H. Anlauf and H. Nirschl[*)]

[*)] Dipl.-Ing. Björn Daumann, Dipl.-Ing. Abdelkrim Fath, Dr.-Ing. Harald Anlauf, Prof.-Dr.-Ing. Hermann Nirschl

University of Karlsruhe (TH), Institute for Mechanical Process Engineering and Mechanics,

Federal Republic of Germany D-76128 Karlsruhe

Tel.:+49721-608-4139, Fax:+49721-608-2403, e-mail: bjoern.daumann@mvm.uka.de

Abstract

This study reports on research results in the field of powder mixing in a discontinuously operated charge mixer. The mixing time for a confidence interval can be determined from the mixing efficiency that characterizes the mixing of the participating solid components as a function of the mixing time. The mixing efficiency is determined here with the help of an image analysis method developed for these purposes. The particle fraction, that is interesting in terms of its distribution, is partially replaced for this purpose by a similarly behaving but optically well identifiable tracer material. A dispersion coefficient can be obtained from the analysis of the mixing trial. The practical application of statistics on image analysis is described and discussed along with a description of the possibilities and limitations of the measurement method. The description of the procedure to determine the dispersion coefficient is built on that.

Keywords: discontinuous powder mixing; mixing efficiency; image analysis; dispersion coefficient; powder sampling

1. Introduction

Mixing of dry or moisturized powders is a unit operation in process engineering processes, and will be found in the construction-, food-, and pharmaceutical industries, as well as in other fields. The user's objective when employing a charge mixer is to attain a defined homogeneity in the solids to be mixed within a shortest possible mixing time. The change in the mixing quality over the mixing time is described by the mixing efficiency. The mixing efficiency is determined in the classical manner, representative solid samples are taken out of the mixing chamber and are analyzed outside for their composition. This procedure of powder sampling is based on a statistic background. Each individual measurement point in the mixing quality curve represents the result of several samples that were taken and whose number is determined by the user. These samples must then be analyzed outside the mixer with a relatively major effort. The more samples are taken out of the mixing chamber, the closer to the expected value will be the result of the concentration measurements. But, as the sample is taken, an always irreversible interference is generated at the sampling site, which action critically influences the surrounding mixture. Systematic

sampling at firmly defined sites is necessary in order to be able to make meaningful comparisons among mixing efficiencies against the background of differing initial states. The described procedure has already been illustrated in detail in the available literature *Raasch et al. (1995)* and *Hauser et al. (1989)*, and it was also discussed and investigated. Just as sampling is done according to the state of the art, the mixing chamber must according to *Koch et al. (1996)* be subdivided systematically into individual segments. By means of a suitable sampler and support by the random generator, the individual samples to be analyzed are selected and removed from the various segments. The samples are then analyzed outside the mixing chamber. If the samples to be analyzed contain components that can harden, then measurement methods used outside the mixing chamber are rather unsuitable. The problem might be solved by optical or also radiometric measurement methods that facilitate the analysis directly in the mixing chamber itself.

We know of experiments that are intended to reduce the effort involved in the reevaluation of continuous/discontinuous powder mixers with the help of modern spectroscopy methods according to *Merz (1973), Holzmüller (1984), Weinekötter (1993), Habermann (2005)* and *Kehlenbeck (2006)*. There exist a lot of more measurement methods like in *Chee-Kong et al. (2002, 2004)*, *Ehrhardt et al. (2005), Hardy et al. (2007)* to estimate powder samples. But these methods are of limited use on account of the limitations of the permissible sample volume. Their calibration constitutes a problem for all measurement methods because any change in the solid system requires a renewed calibration. Errors in the determination of the concentration result if this is not complied with. Most recently, measurement methods have been used in charge mixers where the discontinuous mixer was either completely transilluminated with x-rays or where PEPT-measurements (Positron Emission Particle Tracking) were employed according to *Yang et al. (2004), Ingram et al. (2005)* and *Puyvelde et al. (2006)*. These methods likewise are suitable only for laboratory mixers with limited capacity. Optical measurement methods with fiber optic waveguides and CCD-cameras were used in *Stalder (1993), Metcalfe et al. (1995), Wightman et al. (1996), Khakhar et al. (1997), Muzzio et al. (1997), Eichler (1998), Puyvelde et al. (1999), Aoun-Habbache et al. (2002), Realpe et al. (2003), Ålander et al. (2003), Landwehr (2005)*, *Berthiaux et al. (2006) and Muzzio et al. (2008)*. Here, image analysis was in all cases used for the purpose of characterizing the mixing state. These analysis methods are particularly suitable when one must characterize particles of different color. The above-mentioned authors, that use image analysis for powder mixing, could not always get along without taking samples from the mixing chamber – something that necessarily had to be accompanied each time by brief interruptions of the mixing operation.

The progress in mixing analysis, presented in this study, resides in the development of an image analysis method without sample taking for direct determination of the concentration curve and that the mixing efficiency during the mixing process in the mixing apparatus. A CCD-video camera records the mixing process throughout the entire mixing time so that one can at any time fall back on certain specific sequences and one can generate any number of measurement points for the mixing efficiency. One advantage inherent in this measurement method is represented by the fact that the camera can be adapted in a flexible manner if there is a change in the structural size of the mixer or of the sample volume. Besides, at

all times there is access to the raw data so that one might possibly be able to vary the analysis method. Finally, moved images can, over the time of the entire mixing process, illustratively clarify the procedure going on in the powder mixer.

2. Experimental Apparatuses, Structure of Experiments, and Product Characterization

2.1 Experimental Apparatuses and Structure of Experiments

The experiments were carried out on the horizontal twin-shaft-paddle mixer supplied by Firma ELBA-Werk Maschinen GmbH. According to Fig. 1, the volume of the twin-shaft-paddle mixer is V=120L. The powder mixer is equipped with a spiral mixing tool. The characteristic feature of the twin-shaft-paddle mixer is represented by the fact that the two mixing tools intersect each other in the central part of the mixing chamber. These tools move opposite to each other and convey the product from the outer edge of the trough toward the interior. In the case of the twin-shaft-paddle mixer, the mixing tool running along the wall has a diameter of D_W=550mm. The ratio between the drum diameter and the length is D_T/L≈2. The filling ratio φ corresponds to approximately φ≈50%. The revolutions per minute n can be adjusted phaselessly up to 49rpm. All mixing trials are run at a constant revolutions per minute of n=15rpm. The powder mixer is employed in practice to process concretes and mortar with differing mixing times. In the average mixing runs, the mixing times are approximately t_M≈30 sec according to *Charonnat et al. (1997)*.

The Sony VX2100E video camera used here has a resolution of 720pixels·576pixels with an image rate of 30 images per second. By positioning the video camera perpendicularly above the mixing chamber, one can continuously observe or record the mixing procedure. A 1000-watt halogen lamp so illuminates the mixing chamber that shadow formation by the mixing tool and the trough rim can be greatly reduced according to Fig. 2 and the influence of foreign light can be kept small so that these potential error sources can be disregarded during the analysis.

Figure

Fig. 1. View of the mixing chamber of the twin-shaft-paddle laboratory mixer with spiral mixing tool

Figure

Fig. 2. Side view of the perpendicularly positioned video camera

2.2 Product Characterization for tracking the powder flow

Special color particles (tracer particles) are used for the mixing experiments; these particles could be identified adequately well by means of a definite contrast with respect to the surroundings. Pigments with varying qualities have already been used successfully in other studies of *Collin et al. (2007)* and *Lee et al. (2007)*.

Table 1 shows the particle size of cement x_{50}, ultramarine, and ferrous oxide obtained with the help of laser diffraction. Riboflavin is water soluble, so not sensible for this experiment. It is obvious from the integral distributions Q_3 that both color pigments are distributed closely, where as the cement component is distributed over a wide range. The pigments have been selected, such that the mean particle diameter x_{50} of both products nearly agrees with that of the cement component.

	Riboflavin	ferrous oxide	Ultramarine blue	Cement
Color	Yellow	Red	Blue	Grey
Solid Density ρ_S	2100 kg/m³	5000 kg/m³	2400 kg/m³	2900 kg/m³
Particle Diameter x_{50}	-	5.5 μm	16.2 μm	13.51 μm
Solubility in Water	good till low	No	No	Low

Table 1 pigments for replacing the cement

The cement by table 1 is the component to be marked. The tracer component selected first for the detection of the cement distribution is riboflavin. This solid fluoresces under UV light at low solid concentrations. It was found in preliminary tests that the riboflavin does no longer fluoresce in combination with the cement at a pH value of 13, such that it cannot be used for this type of tracing. pH depending on fluorescence can be found in *Drössler P. et al. (2002)*. Ferrous oxide also is a strongly coloring pigment. When tracing the cement, a high intensity results. However, cleaning of the mixing volume is difficult. Another problem lies in the density difference between ferrous oxide and cement from 2000 kg/m³ till 3000kg/m³. Ferrous oxide has a much higher density that cement according to *Collin et al. (2007)*.

Hence, ultramarine is chosen, as its density; mean particle diameters are very close to those of cement. In accordance with a recommendation of the producer Scholz, a concentration range of $\overline{c_{P,E}}$ =0.5%-1% (related to the total quantity) was employed so that the product properties of the mixing material (compressive strength, flow properties, etc.) would not be influenced impermissibly by the coloration with the pigment. In this described concentration intervals of ultramarine blue compressive strength experiments with typical concrete mixtures were done. Only in the range from $\overline{c_{P,E}}$ =0.5%-1% the compressive strength has a low influence.

The tracer used here is not intended to dye or mark a certain particle fraction. This tracer represents a substitute or filler for the component of interest, in this case cement. The cement thus was replaced by the tracer in order to be able to visualize its mixing behavior with the other components of the model mixture.

4

The mixture investigated here consisted of the tracer and an additional three varying particle fractions in the range of 0.5mm–16mm. Additional data regarding the properties of the model mixture can be gleaned from the literature of *Daumann et al. (2007)*.

The pigment selected here was ultramarine blue because its particles – in terms of density, size, flow behavior, sphericity, and compression behavior - behave very similarly when compared to cement. It was possible to document in prior investigations that the selected material permits an identification in the image analysis program and almost retains its color spectrum. When liquid and other components are added, the color intensity does not display any color changes if the tracer is always uniformly distributed over the entire mixing chamber with progressing mixing time.

According to Table 2, the volume sum distributions $Q_3(x)$ yielded the particular particle sizes x_{10}, x_{50}, and x_{90}. The color pigment displayed a tighter particle size distribution as did the cement. The obtainable size categories had average particle sizes of $x_{50} \approx 1 \mu m$, $x_{50} \approx 5 \mu m$, $x_{50} \approx 15 \mu m$. Because cement has approximately an average particle size of $x_{50} \approx 13 \mu m$, the size class of $x_{50} \approx 15 \mu m$ was selected. The nondimensional parameters Hausner-ratio H and the Carr-Index C can be determined via the determination of the powder density ρ_S, the bulk density ρ_B, the tapped density ρ_T according to *Hausner (1967)* and *Carr (1965)*. These parameters describe the compression behavior of fine powders. Since the Hausner-ratio is $H>1.15$ and since the Carr-Index is $C>25\%$, these – according to the definition of both authors – are bulk materials with restricted flow behavior.

	Ultramarine Blue	Cement
Color	Blue	Grey
Particle diameter x_{10}	10.5μm	2.4μm
Particle diameter x_{50}	16.2μm	13.51μm
Particle diameter x_{90}	20.5μm	82μm
Powder density ρ_S	2400kg/m³	2900kg/m³
Bulk density ρ_B	990kg/m³	1200kg/m³
Tapped density ρ_T	1400kg/m³	1750kg/m³
Hausner-ratio H	1.41	1.45
Carr-Index C (%)	29.3	31.4
Sphericity Ψ	≈ 0.82	≈ 0.78

Table 2 Powder Properties

The sphericity Ψ of both substances, amounting to $\Psi \approx 0.8$, differs only to a slight degree. The flow properties of dry and moist powders were determined according to the analysis method of *Schulze (1995, 1998)* in the Jenike shearing cell. The pertinent measurement results are given in Fig. 3. The shearing site, that represents the shearing stress τ_N plotted against the normal stress σ_N, displays comparable results for the pigment ultramarine blue and cement. The quantity of cement or pigment remained constant while the

share of water was varied. The higher the water/cement ratio became, the more stable was the bulk plotted against the shearing, as a result of the internal friction caused by the increasing capillary adhesion forces. The shearing stress decreased again only at water/cement ratios of $W/C > 25\%$, something that indicates a flow behavior that is improving once again. The cement attained its complete texture saturation at $W/C > 25\%$, and the now freely movable water increased the flowability of the mass. In that case, measurements with the shearing cell are no longer possible.

Figure

Fig. 3. Determination of flow site according to Jenike

3. Theoretical Fundamentals to Determine the Mixing Efficiency by using image analysis

3.1 Processing the digital images and determining the threshold value

The individual digital images have a resolution of 720pixel·576pixel. The blue component therefore cannot be resolved all the way to the primary particle size. But it is possible to get an impression of the mixing quality with a resolution of per sample. The details can be depicted more precisely if the resolution is selected to be considerably higher. Of course, disturbing nonhomogeneities, such as reflections of particles or the formation of shadows, by the mixing tools and the trough rim, can decisively dominate the determined mixing efficiency. The evaluations showed that a resolution of 366.8mm^2 is fully sufficient in order to describe the mixing efficiency with sufficient accuracy. The number of the digital images results from the [number of] images that are recorded by the video camera, per second.

The individual images were so reprocessed in the Adobe Photoshop® CS2 that after the setting of a threshold value, only the blue component remained preserved. In the image analysis, the threshold value defines the differentiability between the tracer and the model mixture. The blue tracer component was separated with the help of the Adobe Photoshop® CS2 image processing program. The threshold value of individual command sequences was defined in the course of prior experiments; these sequences actually should no longer be altered during the actual experiments. It was possible to separate the tracer component by enhancing the tracer color.

3.2 Determination of the mass-concentration by the surface of a powder sample

For the determination of mixing quality s^2 the concentration of the sample N_S is necessary. The target value concentration $\overline{c_{P,E}}$ is then calculated according to Eq. 1.1 from the weigh-in of pigment m_S, the present mass-related moisture $x_W \approx 5\%$, and the total mass (in this case, $m_{m,T}$=200kg) of the main component. According to *Daumann et al. (2007)*, the main component consists of three fractions with almost identical quantitative ratios,

$$\overline{c_{P,E}} = \frac{m_{Pig.}}{m_{Pig.} + (1 + x_W) \cdot m_{m,T}} \approx 0.71\%. \tag{1.1}$$

The information on the local concentration distribution $c_{P,i}$ is lost as a result of the conversion of the digital images into a binary representation without greyscales. This now missing information can be obtained by considering that the tracer component, after being charged into the mixing chamber, will be distributed uniformly with progressing mixing time. The initial concentration of the tracer $\overline{c_P}(t_M = t_0)$=1 changes into the target value concentration $\overline{c_{P,E}}$ as a result of the mixing process and the resultant homogeneous distribution. The maximum acquired surface is assigned here to the total mass. To determine the concentration efficiency in terms of time $\overline{c_P}(t_M)$, according to the provisions of Eq. 1.2, one needs the quotient from the temporal surface change of the blue total surface $A_{B,T}$ and the total surface of the mixing chamber A_T Eq. 1.2 differs from Eq. 1.1 only by virtue of this surface ratio. All of the other magnitudes – such as the mass-related humidity x_W, the total mass of the bulk material $m_{m,T}$, and the total mass of the pigment $m_{Pig.}$ – are preserved,

$$\overline{c_P}(t_M) = \frac{m_{Pig.}}{m_{Pig.} + \dfrac{A_{B,T}}{A_T} \cdot (1 + x_W) \cdot m_{m,T}}. \tag{1.2}$$

The calculated concentration $\overline{c_P}(t_M)$ is assigned to each pixel that is colored black at the mixing moment t_M. The white pixels have a concentration of c_{Pi}=0. If the previously defined samples A_S are evaluated, then a number of pixels in the sample A_S will have the color black, while all others remain white. The concentration c_{Pi} results according to Eq. 1.3 from the product of concentration $\overline{c_P}(t_M)$ and the quotient from the surface of the black pixels $A_{B,S}$ and the total surface of sample A_S. If the sample A_S is completely black, then it has a concentration of $\overline{c_P}(t_M)$. The empirical variance can then be calculated at every mixing moment t_M if one knows the local concentration,

$$c_{P,i} = \overline{c_P}(t_M) \cdot \frac{A_{B,S}}{A_S}. \tag{1.3}$$

3.3 Definition of mixing efficiency

According to *Sommer (1982)*, the mixing efficiency – determined via the time span of the variance $\sigma^2(c_{P,i},t_M)$, according to Eq. 2.1 – consists of three variances. The variance of the measurement method σ^2_M denotes the reproducibility and is obtained from preliminary tests. As a rule, the latter should be so small that only the variance of the uniform random mixture σ^2_Z will influence the system and that the variance of the measurement method σ^2_M is thus negligible ($\sigma^2_Z \gg \sigma^2_M$). The systematic variance σ^2_{Syst} is thus a function of time and, in its stationary state, has the value $\sigma^2_{Syst}=0$, which means that the mixing process is terminated. A longer mixing time does not improve the mixing quality. The systematic variance is diminished during the mixing process by the individual particle size $m_{E,T}$ and the sample quantity m_S.

The variance $\sigma^2(c_{P,i},t_M)$ is calculated by forming the sum of the deviation squares with the target value concentration $\overline{c_{P,E}}$ for the individual samples N_S, as is also given in Eq. 2.1. The mixing efficiency then results from the determination of the variance $\sigma^2(c_{P,i},t_M)$, with differing mixing times. The variance exists only theoretically because its actual determination requires an infinite number of samples N_S. In practice, only a limited number of samples N_S can be studied; therefore, the mixing quality is estimated by means of the empirical variance $s^2(c_{P,i},t_M)$, on the basis of the existing analyzed samples,

$$\sigma^2(c_{P,i},t_M) \approx s^2(c_{P,i},t_M) = \frac{1}{N_S} \cdot \sum_{i=1}^{N_S} \left(c_{P,i} - \overline{c_{P,E}}\right)^2 = \sigma^2_M + \sigma^2_Z + \left(1 - \frac{m_{I,T}}{m_S}\right) \cdot \sigma^2_{Syst.}. \tag{2.1}$$

The variation coefficient v is calculated from the quotient between the square root of the empirical variance according to Eq. 2.1 and the target value concentration $\overline{c_{P,E}}$ (Eq. 2.2),

$$v = \frac{s(c_{P,i},t_M)}{\overline{c_{P,E}}}. \tag{2.2}$$

The mixing process is dispersive while the motion behavior is almost identical; therefore, at the end of the mixing process, the variation coefficient v_Z of the ideal random mixture behaves according to Eq. 3.1. According to *Müller (1966)*, the ideal random mixture is almost always achieved when the particle size distribution is similar. The variation coefficient of the ideal random mixture v_Z is calculated, according to *Stange (1963)*, from the mass of the individual particle $m_{I,T}$, the sample quantity m_S, and the target value $\overline{c_{P,E}}$. For particles that do not have a spherical shape and that do not have a mono disperse particle size distribution, Eq. 3.1 after *STANGE* was so modified in *Daumann et al. (2008)* that the influence of the distribution and the particle shape is considered. The particularly equal-volume diameters $x_{V,T}$ of the tracer or of the equal-surface diameter $x_{A,T}$ can be determined by simple conversions,

$$v_Z = \frac{\sigma_Z}{c_{P,E}} = \sqrt{\frac{\left(1 - \overline{c_{P,E}}\right)}{\overline{c_{P,E}}} \cdot \frac{m_{I,T}}{m_S}} = \sqrt{\frac{\left(1 - \overline{c_{P,E}}\right)}{\overline{c_{P,E}}} \cdot \frac{\rho_S \cdot \frac{1}{6} \cdot \pi \cdot x_{A,T}^2 \cdot x_{V,T} \cdot \psi}{m_S}} \approx 6.75 \cdot 10^{-6}. \tag{3.1}$$

8

The sample quantity m_S can be calculated according to Eq. 3.2. This Equation consists of the sphericity Ψ, the equal-volume diameter of a sphere x_V, the projected surface of the sample A_S, the powder density ρ_S, and the mass concentration c_j of the individual components j in the powder mixture,

$$m_S = \frac{2}{3} \cdot \rho_P \cdot \sum_{j=1}^{N} A_S \cdot c_j \cdot x_{V,j} \cdot \psi \approx 2.8g. \tag{3.2}$$

The variation coefficient of the measurement error v_M according to Eq. 4 can be determined via a defined sample size A_S=15pixel·12pixel, that circumscribes the surface of the largest particle present in the mixture. The result clearly shows that the measurement error of the variation coefficient dominates the result because the latter is greater than the variation coefficient of the ideal random mixture v_Z. In determining the variation coefficient v, one must therefore consider both the variance of the ideal random mixture σ^2_Z and the variance of the measurement method σ^2_M,

$$v_M = \frac{\sigma_M}{c_{P,E}} = \frac{A_{I,S}}{A_S} = \frac{1Pixel \cdot 1Pixel}{15Pixel \cdot 12Pixel} \approx 5.56 \cdot 10^{-3}. \tag{4}$$

The variation coefficient of the so-called zero mixture σ^2_0 according to Eq. 5, a completely demixed state of a twin-component mixture, is also calculated from the target value concentration $\overline{c_{P,E}}$,

$$v_0 = \frac{\sigma_0}{c_{P,E}} \sqrt{\frac{\left(1 - \overline{c_{P,E}}\right)}{\overline{c_{P,E}}}} \approx 11.83. \tag{5}$$

3.4 Determining the empirical variance from the digital images

According to the processing in Photoshop the resultant digital image is read into the Matlab[®] Image Processing Toolbox as a 720pixel·576pixel·3 (color) matrix. The analysis algorithm can be found in Fig. 4. 720pixel·576pixel·3 (color) matrix is generated by Matlab[®] after the color digital image has been read into the Matlab[®] Image Processing Toolbox. This matrix is then converted into a binary digital image (black/white). During the conversion, of course, no grey-scale digital image was generated because prior tests revealed that it is impossible to determine a concentration from the grey scales.

Figure

Fig. 4. Analysis algorithm for the determination of the mixing efficiency and the concentration efficiency

After the digital image has been read into Matlab[®], it is subdivided into individual segments that correspond to a sample size of 15pixel·12pixel. That yields a number of samples of N_S=576 for a 720pixel·576pixel digital image. Shadow formation on the trough rim and the imaging of the mixing tools are not considered because, when it comes to calculating the empirical variance, one uses only samples with 15pixel·12pixel from the middle part of the mixing chamber. The total matrix of 48·48 samples, with a resolution of 720pixel·576pixel, is thus reduced to a segment of 24·24 samples.

An additional data reduction is necessary to reduce the computing effort. This is achieved in that no more than two digital images are analyzed within one second of mixing time. That reduces the entire computation time from thirty minutes to two minutes. Another computation time reduction results from a reduction of the number of samples from N_S=576 to N_S=120. The samples are selected with the help of a binary random generator (type of random matrix), that is integrated into the Matlab[®] Communications Toolbox.

The empirical variance s^2 is determined from the concentration field after the statistical selection of 120 samples. This statistical selection of the sample should avoid additional variability of the concentrations. The procedure is comparably with a rotary sample splitter or riffle splitter by free flow powders. According to Eq. 6.1, the individual differences of concentration $c_{P,i}$ and the target value $\overline{c_{P,E}}$ are summated in a square fashion. The target value concentration $\overline{c_{P,E}}$ is then calculated according to Eq. 1.1,

$$s^2 = \frac{1}{120} \cdot \sum_{i=1}^{120} \left(c_{P,i} - \overline{c_{P,E}} \right)^2 . \tag{6.1}$$

The mixing efficiency can then be illustrated by plotting the variation coefficient against the mixing time t_M. Fig. 5 shows the concentration field developing on the mixer surface. The reduction of the matrix from 48·48 samples to 24·24 samples has additionally been recorded there,

Figure

| (a) | (b) | (c) |

Fig. 5. Determination of the concentration field on the mixer surface (a) binary digital image, (b) concentration field without reduction, (c) concentration field with reduction

The variation coefficient v is determined according to Eq. 6.2. The quotient from the root of the empirical variance s^2 according to Eq. 6.1 and the target value concentration $\overline{c_{P,E}}$ then yields the relative deviation,

$$v = \frac{s}{\overline{c_{P,E}}} . \tag{6.2}$$

3.5 Determining the confidence interval

With the help of the χ^2-distribution, one can evaluate the extent to which the measured variation coefficients v yield statistically secure measurement values. The χ^2-distribution presents an upper and lower confidence interval within whose boundaries the variation coefficient should lie with a certain degree of probability, according to Eq. 7. The variances of the ideal random mixture are to be calculated with σ^2_Z and those of the measurement error are to be calculated as σ^2_M, with the help of Eq. 1.1, Eq. 3.1 and Eq. 4. The sample size here is designated N_S. The χ^2-values from the χ^2-frequency distribution are calculated for an

information correctness probability of α=99.99%. This procedure for powder mixtures is explained very precisely in *Pahl et al. (1992)*,

$$\frac{\sqrt{\dfrac{\chi^2_{UB} \cdot (N_s - 1, \alpha)}{N_s - 1} \cdot (\sigma^2_Z + \sigma^2_M)}}{\overline{c_{P,E}}} = v_{UB} \leq \frac{s}{\overline{c_{P,E}}} = v \leq \frac{\sqrt{\dfrac{\chi^2_{OB} \cdot (N_s - 1, 1 - \alpha)}{N_s - 1} \cdot (\sigma^2_Z + \sigma^2_M)}}{\overline{c_{P,E}}} = v_{OB} \quad (7)$$

$$\frac{\sqrt{\dfrac{\chi^2_{UB} \cdot (N_s - 1, \alpha)}{N_s - 1} \cdot \left([v_Z \cdot \overline{c_{P,E}}]^2 + [v_M \cdot \overline{c_{P,E}}]^2\right)}}{\overline{c_{P,E}}} = v_{UB} \leq \frac{s}{\overline{c_{P,E}}} = v \leq \frac{\sqrt{\dfrac{\chi^2_{OB} \cdot (N_s - 1, 1 - \alpha)}{N_s - 1} \cdot \left([v_Z \cdot \overline{c_{P,E}}]^2 + [v_M \cdot \overline{c_{P,E}}]^2\right)}}{\overline{c_{P,E}}} = v_{OB} \,.$$

3.6 Determination of the dispersion coefficient from the mixing efficiency

The literature on powder mixing offers a whole series of models for the description of the mixing efficiency. The models are divided in models for continuous powder mixing and charge powder mixing. Some model statements can be used for continuous and discontinuous powder mixing. In the text the most common model will be responded.

A model presentation for continuous mixing involves the subdivision of the powder mixer into many small stirring vats and thus corresponds to the so-called stirring vat cascade model. This model has been used to describe continuous mixers by *Weinekötter (1993)* and *Habermann (2005)*.

More recent publications propose statistical and numerical statements, such as Markov-chains or the discrete Element Model (DEM) (*Aoun-Habbache et al. (2006)* and *Bertrand (2005)*). The models are very demanding depending upon the computation accuracy and the number of particles. These models have their application in continuous and charge powder mixing.

The FAN model according to *Wang et al. (1976)* for example represents a modification of the even simpler model of *Rose (1959)*. Both models have the same structure and concept. This statement is based on a 1st-order reaction equation. The resultant exponential function with two fitting constants corresponds to the solutions for chemical process engineering.

Many authors use the FOKKER-PLANCK-equation that can be used both with charge mixers and with continuous mixers (*Müller (1966), Hogg et al. (1966), Sommer (1979), Fan et al. (1990), Habermann (2005) and Kehlenbeck (2006)*). This equation will be covered in greater detail below. The concept by using this equation is very simply to handle. The equation makes it possible to adapt a statistic concept without fitting or correction parameters.

Eq. 8.1 according to *Müller (1966)* is also called the 2nd Kolmogorov-equation. The particle movement is random and has no after effects, the prior history does not influence the process. Such a process is also referred to as the Markov-process,

$$\frac{\partial c_P}{\partial t_M} = D \cdot \frac{\partial c_P{}^2}{\partial^2 x} - T \cdot \frac{\partial c_P}{\partial x}. \tag{8.1}$$

The FOKKER-PLANCK-equation according to Eq. 8.1 is a function of the Site x and the mixing time t_M. The partial differential equation contains a dispersion term and a convection term. The dispersion term

describes the concentration adjustment in the powder system by means of the dispersion coefficient D. The transport term, with the transport coefficient T, characterizes the influence of the selected transport of the particles. It describes a demixing of the system in case of varying movement behaviors of the particles. The analytical solutions to these equations make it possible to determine the dispersion coefficient D according to *Müller (1966)*, after neglecting the transport term T. But very few solutions are known where the transport term is given consideration according to *Fan et al. (1990)*. The severe dependence of the dispersion coefficients D from the powder qualities makes it hardly possible to separate from the dispersive distribution and the convective transport procedures. The reason for this strong dependence, according to Müller (1966), is that the dispersive distribution of the particles is subjected to external influences. Therefore, the dispersion coefficients in charge mixers as a rule is construed as a summary magnitude and the transport coefficient is neglected according to *Müller (1966), Hogg et al. (1966), Fan et al. (1979)* and *Sommer (1979)*. This assumption however is justified only if the particle properties do not differ too much from each other in terms of their movement behavior. The particles move in different ways, one encounters demixings in the powder bulk material which become recognizable according to *Sommer (1979)* in the mixing efficiency in the form of deviations from the ideal random mixture. In continuous mixtures, the transport term is equated to the speed of the mixing tool according to *Habermann (2005)*. The FOKKER-PLANCK-equation is well suitable for describing the mixing efficiency to the extent that only one single adaptation magnitude is contained in it. When almost identical experimental conditions and products are presumed, the dispersion coefficient can be used as a measure of the mobility of a particle in a powder bulk pile.

A unidimensional solution can be given according to *Müller et al. (1966)*, by the Fokker-Plank -equation, if one assumes a stochastic mixing process. Eq. 8.2 presents the concentration efficiency $c_P(x,t_M)$ in terms of time as a function of the dispersion coefficient D, the mixing time t_M, and the length L. This equation is appointed to the initial and boundary conditions. The components are fully separated at the beginning of the mixing procedure at $t_0=0$ through a barrier with the length L_0. During the powder mixing process the boundaries of the mixer at the positions at x=0 and x=L don't show any gradients,

$$c_P(x,t_M) = \overline{c_{P,E}} + \frac{2}{\pi} \cdot \sum_{v=1}^{\infty} \cdot \frac{1}{v} \cdot sin\left(v \cdot \pi \cdot \overline{c_{P,E}}\right) \cdot cos\left(v \cdot \pi \cdot \frac{x}{L}\right) \cdot exp\left(-v^2 \cdot \left(\frac{\pi}{L}\right)^2 \cdot D \cdot t_M\right). \tag{8.2}$$

boundary conditions for Eq.8.1 : $\dfrac{\partial c_P(0,t_M)}{\partial x} = 0$ $\dfrac{\partial c_P(L,t_M)}{\partial x} = 0$

initial conditions for Eq.8.1 : $c_P(x,t_0) = 1$ *for* $0 \le x \le L_0$

                                         $c_P(x,t_0) = 0$ *for* $L_0 \le x \le L$

If the mixing time $t_M \gg t_0$, the concentration $c_P \ll 1$ and the higher terms of $v > 1$ are neglected then Eq. 8.2 can be simplified according to the following Eq. 8.3,

$$c_P(x,t_M) = \overline{c_{P,E}} \cdot \left(1 + 2 \cdot \cos\left(\frac{\pi}{L} \cdot x\right) \cdot \exp\left(-\left(\frac{\pi}{L}\right)^2 \cdot D \cdot t_M\right)\right). \tag{8.3}$$

After an integration of Eq. 8.3, we get Eq. 8.4 for the systematic variation coefficient $\sigma^2_{Syst.}$ Eq. 8.5 follows by inserting the magnitudes from Eq. 8.4 in Eq. 2.1. Only the systematic variance $\sigma^2_{Syst.}$ is a function of the mixing time. We get the variation coefficient v, according to Eq. 8.6, if the root of the empirical variance is related to the target value concentration,

$$\sigma^2{}_{syst.} = \frac{1}{L} \cdot \int_0^L \left(c_P(x,t_M) - \overline{c_{P,E}}\right)^2 \cdot dx = \sigma_0^2 \cdot \exp\left(-\left(2 \cdot \left(\frac{\pi}{L}\right)^2 \cdot D \cdot t_M\right)\right), \tag{8.4}$$

$$\sigma^2\left(\overline{c_{P,E}}, t_M\right) = \sigma^2{}_z + \sigma^2{}_M + \left(1 - \frac{m_{I,S}}{m_S}\right) \cdot \sigma^2{}_0 \cdot \exp\left(-\left(2 \cdot \left(\frac{\pi}{L}\right)^2 \cdot D \cdot t_M\right)\right), \tag{8.5}$$

$$v = \frac{\sigma\left(\overline{c_{P,E}}, t_M\right)}{c_{P,E}} = \frac{\sqrt{\sigma^2\left(\overline{c_{P,E}}, t_M\right) = \sigma^2{}_z + \sigma^2{}_M + \left(1 - \frac{m_{I,S}}{m_S}\right) \cdot \sigma^2{}_0 \cdot \exp\left(-\left(2 \cdot \left(\frac{\pi}{L}\right)^2 \cdot D \cdot t_M\right)\right)}}{\overline{c_{P,E}}}. \tag{8.6}$$

The only magnitude that is as yet unknown in Eq. 8.6 is the dispersion coefficient D. Both the sample quantity m_S, and also the individual particle size of the tracer $m_{I,T}$, the variance of the random mixture σ^2_z, the variance of the measurement error σ^2_M, the variance of the zero mixture σ^2_0, and the target value concentration $\overline{c_{P,E}}$ can be gathered from the interrelationships in Chapter 3.2 till 3.4. One can determine the dispersion coefficient D from the mixing efficiency according to Eq. 8.7 as a result of the conversion of Eq. 8.6. The dispersion coefficient is determined by linear regression. It is suitable as comparison magnitude for differing marginal values, products, and experimental conditions,

$$\frac{ln\left(\frac{\sigma^2\left(\overline{c_{P,E}}, t_M\right) - \sigma^2{}_z - \sigma^2{}_M}{\left(1 - \frac{m_{I,S}}{m_S}\right) \cdot \sigma_0{}^2}\right)}{2 \cdot \left(\frac{\pi}{L}\right)^2} = -D \cdot t_M. \tag{8.7}$$

3.7 Limitations on image evaluation and of the model

The practical determination of the mixing efficiency by means of image analysis presumes that the mixing chamber offers adequate accessibility for the use of the video camera from above and that there is almost no influence from outside light. The chosen sample size must not be too small because otherwise the measurement error will dominate the analysis. The mixing tool should permit three-dimensional transport. This analysis method cannot be used for startup procedures in case of mixing times of less than two seconds; this will be made quite clear in the subsequent discussion of the experimental results. This is

explained by the analysis that takes place exclusively on the surface of the mixing material, something that presupposes a statistical mixing process without any prior history. The resultant surface concentration profile, at the start of the mixing process, does not agree with the concentration distribution in the total volume of the mixture.

The limitations on the FOKKER-PLANCK-equation for the description of the practical case covered here, in addition to the presumption of a stochastic mixing process, includes the disregarded selected transport (demixing) of the various components contained in the mixture. The dry products display severe demixing phenomena during the mixing process according to *Daumann et al. (2008)*, something that adds up to a selective mixing behavior. A selected mixing behavior on the part of the powder particles can be observed in *Daumann et al. (2007)* as a result of the freely movable liquidity of the suspension which is then present, also in capillary liquid saturations of S>1. That can also be expected when working with very high mass-related humidities, as in the case of bulk materials used here, amounting to x_W>7.5%. These boundary cases cannot be described with the FOKKER-PLANCK-equation that presupposes a pure dispersion. One may assume that the mixing behavior will be dispersive if the powder bulk pile has an almost homogeneously distributed humidity in the range of 0%>x_W<7.5%. The mixings were found according to *Daumann et al. (2007)* only in the boundary area of the ideal random mixture. Image analysis is dominated by the measurement error in the homogeneous mixing range; therefore, the demixings, covered in *Hoffmann (1995)* and *Daumann et al. (2007)* and, do not have any influence on the evaluation. The determined empirical variance connected with the experiments that were performed does not correspond to an empirical volume/mass variance but rather to a surface variance. In the course of experiments, *Debbas (1965)* was able to prove that the two variances should be evaluated equally if there are no demixings from the height, if a random process/package is present, and if the entire collective, consisting of several cutting planes, can be combined into a total variance.

4. Experimental Results and Discussion

To limit the scope of experiments used to determine the mixing efficiency, one keeps constant the revolutions per minute n, filling ratio φ, the pigment concentration c_P, the product composition (model mixture), and the mass-related humidity. Each of these influencing magnitudes has a more or less intensive effect on the mixing times, something that can also be gathered by the literature published on that score *Pahl et al. (1993)*. According to *Daumann et al. (2007)*, it was observed that the arrangement of components in the initial mixture does exert influence; therefore, the components of the model mixture consisting of the three particle fractions were always arranged in the same sequence. The three fractions were positioned horizontally in the mixer according to Fig. 6, whereby, first of all, the finest particle fraction was covered up with the average fraction and the latter was finally covered by the coarsest particle fraction.

14

Figure

Fig. 6. Initial condition of the three moisten particle fractions without zero mixture from tracer

All of the mentioned measures definitely reduced the required number of experiments. The model components were moistened prior to storage in the mixer, individually, during a mixing time t_M of 30-40 seconds, in a separate powder mixer, and the desired humidity of x_W=5% was set for all three fractions of the model mixture. The variation of the charge site of the tracer component is during the experiments the only variation of parameter during the determination of the dispersion coefficient. If this variation of one parameter gives replicable more variation of parameter can measure with this measurement equipment.

A total of three very informative mixing efficiencies were selected from the total number of experiments with different tracer charge sites. Fig. 7 illustrates the variant of the zero mixture with horizontal charge in the form of a diagram. The concentration change in the mixture in terms of time resulted on the basis of the total mixing surface from the binary digital images. The concentrations could be determined for the black image pixels from Eq. 1.2 (see Chapter 3.2). After about 4-6 seconds it was possible to assume that the pigment was subjected to a purely dispersive mixing transport because the anticipated value of the total surface had been attained. Any further concentration adjustment can take place only as a result of dispersion. The fluctuations in the total blue mixing surface, caused by the formation of shadows on the trough rim and the mixing tools, explained the inconstant drop of the concentration curve.

Figure

Fig. 7. Concentration efficiency about the mixing time in the twin-shaft-paddle mixer, starting with the zero mixture

A better indicator to distinguish purely dispersive powder mixing and mixing with transport and dispersion, is the description of the concentration versus dimensionless length $\xi=x/L$. Fig. 8 demonstrates the concentration efficiency over the dimensionless length of the mixer shaft. With progressing mixing time t_M, the tracer will be better distributed in the solid material. After six seconds mixing time, the powder mixing process has subjected to a purely dispersive mixing transport. The high peaks of concentration by mixing time one and three seconds, mark that the mixing equipment transported ultramarine blue temporary on the surface. In the next time steps the pigment disappears in the solid material. The wavelike concentration efficiency by mixing times smaller than five seconds could be explained by the three dimensional movement of the mixing equipment which shows that the transport mechanism still exists.

Figure

Fig. 8. Concentration efficiency about the dimensionless length in the twin-shaft-paddle mixer, starting with the zero mixture

The mixing time can be determined by means of the imaging measurement method during the mixing experiments that were performed. According to the solution of FOKKER-PLANCK, the dispersion coefficient represents a constant magnitude when no product changes occur. The differently measured dispersivities in the subsequent sections spring from the fact that the machine parameter (length L of the concentration adjustment) was altered. That changes the mixing time but not the mobility (dispersion coefficient) of the powder mixing system.

Figure

Fig. 9. Mixing efficiency of the twin-shaft-paddle mixer, starting with the zero mixture, Samples N_S=120, m_S=2.8g, D=232.6cm^2/s

The results from the FOKKER-PLANCK-equation were entered in all mixing efficiency diagrams. Other lines in the mixing efficiencies represent the confidence interval and the variation coefficient of the measurement error. The point recorded for the mixing moment t_M=0, according to Eq. 5, represents the value of the zero mixture. By defining the samples using image analysis method in chapter 3.1 till 3.4, we achieve the mixing efficiency. The horizontal zero mixture shows that, after a relatively short mixing time of t_M≈12-14 seconds, the homogeneous terminal state has been attained. The fluctuation of the curve in the diagram shown in Fig. 9 was caused by the shadows formed by the rotating mixing tools; this is because, due to rotation, a differently sized portion of the mixing surface was available for the evaluation.

Figure

Fig. 10. Mixing efficiency of the twin-shaft-paddle mixer, starting with the zero mixture, Samples N_S=120, m_S=2.8g, D=189.7cm^2/s

If the tracer is not charged horizontally but rather vertically, then, according to Fig. 10, the mixing time is extended from t_M≈12-14 seconds to t_M≈18-20 seconds. This result can also be recognized by virtue of the reduction of the dispersion coefficient D from D≈230cm^2/s to D≈190cm^2/s. The lower the dispersion coefficient, the longer will be the mixing time until a homogeneous terminal state has been reached.´

Figure Table 3		(a) horizontal Tracer charge	(b) vertical Tracer charge
	①	245.6cm²/s ± 22cm²/s	41.9cm²/s ± 7cm²/s
	②	236.6cm²/s ± 24cm²/s	189.7cm²/s ± 15cm²/s
	③	245.1cm²/s ± 21cm²/s	50.0cm²/s ± 5cm²/s

Table 3 Dispersion coefficients in relation to differing zero mixture charges, (a) side view of zero mixtures, (b) top view of zero mixtures

The position of the zero mixture was varied in voluminous experiments (number of experiment per marking $N \geq 3$) and the particular dispersion coefficient was determined from the resultant mixing efficiencies. Table 3 shows the axial mixing process (vertical tracer charge) of the pigment was by up to a factor of five slower than the radial mixing transport (horizontal tracer charge). The homogeneity takes hold considerably faster when the powder components are charged in the horizontal direction.

In case of a horizontal zero mixture, the dispersion coefficients were almost on the same order of magnitude. The radial mixing process was so fast that one could not determine any noteworthy influence from the height. When the zero mixture was charged vertically, the length of the mixture influenced the dispersion coefficient and thus also the mixing time. It turns out that the various vertical tracer charges resulted in a differently fast concentration adjustment. The coloration of the surface, in case of charge (b) ②, was four times faster than charge (b) ③ and (b) ①.

$$D_1 \approx \frac{1}{4} \cdot D_2 \; \left(measurements : D_1 = 41.9 cm^2/s, \, D_2 = 189.7 cm^2/s \right)$$

$$\sigma^2{}_{Syst.1} \sim exp\left(-\left(2\cdot\left(\frac{\pi}{L_1}\right)^2 \cdot D_1 \cdot t_{M_1}\right)\right), \; \sigma^2{}_{Syst.2} \sim exp\left(-\left(2\cdot\left(\frac{\pi}{L_2}\right)^2 \cdot D_2 \cdot t_{M_2}\right)\right),$$

$$L_1 = L, \; L_2 = \frac{1}{2}\cdot L, \; D_1 = D_2 = D,$$

$$\sigma^2{}_{Syst.1} = \sigma^2{}_{Syst.2},$$

$$t_{M_1} \cdot \frac{D_1}{L_1{}^2} = \frac{D_2}{L_2{}^2}\cdot t_{M_2} = \frac{D}{L^2}\cdot t_{M_1} = 4\cdot\frac{D}{L^2}\cdot t_{M_2},$$

$$t_{M_1} = 4\cdot t_{M_2},$$

$$D_1 \sim \frac{1}{t_{M_1}}, D_2 \sim \frac{1}{t_{M_2}}$$

$$D_1 = \frac{1}{4}\cdot D_2. \tag{9}$$

Eq. 8.6, used to determine the dispersion coefficient from Eq. 8.7, among other things, contains the length L of the mixer. The length L was not changed in the analysis algorithm according to Fig. 4. In Eq. 9, the systematic variance $\sigma^2{}_{Syst.}$ for both different mixing times t_{M_1} and t_{M_2} is kept constant. Under condition (b) ②, the concentration adjustment segment is only half as long as in condition (b) ①. The mixing time

17

t_{M_1} is four times longer than the mixing time t_{M_2}. Therefore, according to Eq. 9, one can now explain the four times greater dispersion coefficient D_1 for a tracer marking.

One gets a similar result when the dispersion coefficients (a) ① till (a) ③ are compared to the dispersion coefficients according to (b) ① to (b) ②. According to Eq. 10, as in Eq. 9, this is a function of the concentration adjustment length L. At a filling level of $\varphi \approx 50\%$, the concentration adjustment length roughly corresponds to the radius of the mixing tools. The following relationship is obtained according to Eq. 10, if the dispersion coefficients measured during horizontal tracer charge are formed from an arithmetic mean value:

$$D_1 \approx \frac{1}{5} \cdot D_1 \left(measurements : D_1 = 41.9 cm^2 / s, D_3 = \frac{1}{3} \cdot \left(245.6 cm^2 / s + 236.6 cm^2 / s + 245.1 cm^2 / s\right) = 242.4 cm^2 / s \right)$$

$$\sigma^2{}_{Syst.1} \sim exp\left(-\left(2 \cdot \left(\frac{\pi}{L_1}\right)^2 \cdot D_1 \cdot t_{M_1}\right)\right), \quad \sigma^2{}_{Syst.3} \sim exp\left(-\left(2 \cdot \left(\frac{\pi}{L_3}\right)^2 \cdot D_3 \cdot t_{M_3}\right)\right),$$

$$L_1 = L = 600 mm, \quad L_3 = \varphi \cdot D_W = \frac{1}{2} \cdot 550 mm, \quad D_1 = D_3 = D,$$

$$\sigma^2{}_{Syst.1} = \sigma^2{}_{Syst.3},$$

$$t_{M_1} \cdot \frac{D_1}{L_1{}^2} = \frac{D_3}{L_3{}^2} \cdot t_{M_3} = \frac{D}{(600 mm)^2} \cdot t_{M_1} = \frac{D}{(0.5 \cdot 550 mm)^2} \cdot t_{M_3},$$

$$t_{M_1} \approx 5 \cdot t_{M_3} = 5 \cdot t_{M_3},$$

$$D_1 \sim \frac{1}{t_{M_1}}, D_3 \sim \frac{1}{t_{M_3}}$$

$$D_1 = \frac{1}{5} \cdot D_3.$$

(10)

The result shows that the differently measured dispersion coefficients in reality correspond to differently long mixing times, which are a function of the length. The dispersivity does not represent any change in magnitude, assuming the product qualities remain the same.

If the tracer component according to the zero mixture (a) ① is homogeneously distributed over the surface, then it was found that an analysis on the mixing surface was successful only if the tracer component had already been distributed for between two and five seconds. The known mixing efficiency according to Fig. 11 takes shape only then. The $D \approx 250 cm^2/s$ dispersion coefficient corresponded to the dispersion coefficient of the other horizontal zero mixtures.

Figure

Fig. 11. Mixing efficiency of the twin-shaft-paddle mixer, starting with the zero mixture, Samples N_S=120, m_S=2.8 g, D=245.6 cm^2/s

The determination of the dispersion coefficients shows that the presented measurement method can be used in order to determine the necessary mixing time with a relatively minor experimental effort when working with a charge mixer. This naturally is possible only if a suitable tracer has been found. The mixing chamber must be accessible to the video camera and the mixing tool must generate a three-dimensional mixing

transport. On the basis of the methodology presented here, the user can determine the dispersion coefficients which will then permit comparisons between powder mixers of different structural size, products, or mixing principles under differing initial states.

Summary

This study reports on powder mixing, using a twin-shaft-paddle mixer. The homogeneity of the mixing material is evaluated by means of the mixing efficiency in this charge mixer. The mixing efficiency is determined here not from the samples that were taken, but by means of an imaging measurement method. The components of interest here are replaced by an optically acquirable tracer. The individual digital images, taken during the mixing process, can be analyzed via the Matlab[®] Image Processing Toolbox and the mixing efficiency can be determined from that. The experimental results are evaluated on the basis of known statistical interrelationships for powder mixing. The mixing efficiency can be calculated, assuming that dispersion coefficients are known, by means of the FOKKER-PLANCK-equation. This coefficient is determined from the experimental results. It is a characteristic comparison magnitude for the particular employed mixer and the product used, if the initial states of the mixing process are to be varied. The position of the tracer in the zero mixture was varied here, in that it was charged both horizontally and vertically. In that way, it was possible to test for its plausibility and effectiveness, the measurement method described here for the determination of the mixing efficiency. The method presented here can be used to supply appropriate data on the mixing efficiency of a component from a multi-component mixture if one considers the limitations inherent in the measurement method.

Acknowledgement

19

Symbols

$A_{B,T}$	Area of the total blue surface of the mixing chamber [pixel^2]
$A_{B,P}$	Area of the blue surface [pixel^2]
A_T	Total surface of mixing chamber [pixel^2]
$A_{I,P}$	Individual pixel surface [pixel^2]
A_S	Sample size [pixel^2]
C	Carr-Index [%]
c_j	Concentration of powder component j [-]
$\overline{c_P}(t_M)$	Target concentration of pigment for mixing time t_M [-]
$\overline{c_{P,E}}$	Target value pigment concentration [-]
$c_{P,i}$	Pigment concentration of one sample i [-]
D	Dispersion coefficient [m^2/s]
D_T	Drum diameter [m]
D_W	Tool diameter [m]
H	Hausner-ratio [-]
j	Sample of image surface [-]
L	Length of mixer [m]
m_S	Sample quantity [kg]
$m_{I,T}$	Mass of the individual grain of the tracer [kg]
$m_{Pig.}$	Mass of the pigment [kg]
$m_{m,T}$	Mass of main component [kg]
n	revolutions per minute [min^{-1}]
N_S	Number of samples [-]
Q_3	Volume distribution [%]
V	Volume of mixer [m^3]
S	liquid saturation [-]
s^2	Empirical variance [-]
t_M	Mixing time [s]
W/C	Water-cement value [-]
x	Distance [m]
x_{10}	Average particle diameter at Q_3=10% value [m]
x_{50}	Average particle diameter at Q_3=50% value [m]
x_{90}	Average particle diameter at Q_3=90% value [m]
$x_{A,T}$	Equal-surface particle diameter of a sphere of tracer [m]
$x_{V,T}$	Equal-volume particle diameter of a sphere of tracer [m]
x_V	Equal-volume sphere [m]

x_W	Mass-related humidity [%]

Greek Symbols

α	Data correctness probability [-]
φ	Filling ratio [-]
χ^2	Chi-square of frequency distribution [-]
ν	Variation coefficient [-]
ν_M	Variation coefficient of measurement error [-]
ν_0	Variation coefficient of zero mixture [-]
ν_{UB}	Lower boundary of confidence interval [-]
ν_{OB}	Upper boundary of confidence interval [-]
ν_Z	Variation coefficient of the ideal random mixture [-]
ξ	dimensionless length [-]
ρ_B	Bulk material density [kg/m^3]
ρ_S	Powder density [kg/m^3]
ρ_T	Tapped density [kg/m^3]
σ_N	Normal stress [N/mm^2]
σ^2	Variance [-]
σ^2_0	Variance of zero mixture [-]
$\sigma^2_{Syst.}$	Systematic variance [-]
σ^2_M	Variance of measurement value [-]
σ^2_Z	Variance of uniform random mixture [-]
τ	Shearing stress [N/mm^2]
Ψ	Sphericity [-]

References

Ålander, E. M., Uusi-Penttilä, M. S. and Rasmuson, Å. C., (2003). Characterization of paracetamol agglomerates by image analysis and strength measurement. Powder Technology, 130, 298-306

Aoun-Habbache M., A. M., Berthiaux H., Mizonov V. (2002). An experimental method and a Markov chain model to describe axial and radial mixing in a hoop mixer. Powder Technology 128, 159-167

Berthiaux H., M. V., Tomczak L., Gatumel C., Demeyre J.F. (2006). Principal component analysis for characterising homogeneity in powder mixing using image processing techniques. Chemical Engineering & Processing 45, 397-403

Bertrand F., Leclaire L.-A. and Levecque G. (2005). DEM-based models for the mixing of granular materials, Chemical Engineering Science 60, 2517-2531

Carr R.L. (1965). Evaluating flow properties of solids. Chem. Eng. 18, 163–168.

Charonnat Y., Beitzel H. (1997). Efficiency of concrete mixers towards qualification of mixers, Materials and structures 30, 28-32

Chee-Kong Lai, C.C. (2002). Application of a fluorescence sensor for miniscale on-line monitoring of powder mixing kinetics. Journal of Pharmaceutical Sciences 93, 60-70

Chee-Kong Lai, Miller B., Katstra WE, Cima MJ, Cooney CL. (2004). Nondestructive and Online Monitoring of Tablets Using Light-Induced Fluorescence Technology. AAPS Pharmscitech Journal 5, 1-10

Chia-Yi Yang, X.-Y. F. (2004). Development and validation of a material-labeling method for powder process characterization using X-ray computed tomography. Powder Technology 146, 10-19

Collin V., Je´ze´quel P. H. (2007). Mixing of concrete or mortars: Dispersive aspects. Cement and Concrete Research 37, 1321-1333

Drössler P., H. W., Penzkofer A., Hegemann P., (2002). pH dependence of the absorption and emission behaviour of riboflavin in aqueous solution. Chemical Physics, 282, 429-439

Daumann B., Nirschl H. (2007). Einfluss der Mischtechnik auf trockene und feuchte Feststoffschüttungen, Influence of the mixing system on dry and moist bulk solids. AT Aufbereitungstechnik/Mineral Processing 48, 19-33

Daumann B., Nirschl H. (2008). Assessment of the mixing efficiency of solid mixtures by means of image analysis. Powder Technology 182, 415-423

Debbas S. (1965). Über die Zufallsstruktur von Packungen aus kugeligen oder unregelmäßig geformten Körnern. Dissertation Universität (TH) Karlsruhe

Eichler P. (1998). Analyse, Modellierung und Optimierung von Schwerkraftmischern. Dissertation Universität Kaiserslautern

Ehrhardt N., Montagne M., Berthiaux H., Dalloz-Dubrujeaud B., Gatumel C. (2005). Assessing the homogeneity of powder mixtures by online electrical capacitance 44, 303-313

Fan L. T., Shin. S. H. (1979). Stochastic diffusion model of non-ideal mixing in a horizontal drum mixer. Chemical Engineering Science 34, 811-82

Fan L.T., Chen Yi-ming and Lai F. S. (1990). Recent Developments in solids mixing, Powder Technology 61, 255-287

Fokker A. D. (1914). Die mittlere Energie rotierender elektrischer Dipole im Strahlungsfeld. Annalen der Physik 348, 810-820

Habermann R. (2005). Untersuchung zur Verknüpfung von Verweilzeit-Verteilung und Mischgüte in einem kontinuierlichen Pflugscharmischer. Dissertation Universität Paderborn

Hardy Edme H., H. J. a. K. G. (2007). The mixing state of fine powders measured by magnetic resonance imaging. Powder Technology 177, 12-22

Hauser G., K. T., Sommer K. (1989). Bestimmung der Mischzeit eines Schaufelmischers mit Schnellentleerung für die Herstellung von Trockenmörtel und Putz, Determination of mixing times of paddle mixer with rapid discharge for production of dry mortar and plaster. AT Aufbereitungstechnik/Mineral Processing 30, 367-374

Hausner H. (1967). Friction conditions in a mass of metal powder. International Journal of Powder Metallurgy 3, 7–13.

Hoffmann T. (1995). Mischen und Befeuchten von Schüttgütern. Dissertation Universität Paderborn

Hogg R., C. D. S., Healy T. W., Fuerstenau D. W. (1966). Diffusional mixing in an ideal system. Chemical Engineering Science 21, 1025-1038

Holzmüller R. (1984). Untersuchung zur Schüttgutbewegung beim kontinuierlichen Feststoffmischen. Dissertation Universität Stuttgart

Ingram A., J. P. K. S., D.J. Parker, X. Fan, R.G. Forster (2005). Axial and radial dispersion in rolling mode rotating drums. Powder Technology 158, 76-91

Kehlenbeck V. (2006). Continuous dynamic mixing of cohesive powders. Dissertation TU München

Khakhar, D. V., McCarthy, J. J., Shinbrot, T. and Ottino, J. M., (1997). Transverse flow and mixing of granular materials in a rotating cylinder. Physics of Fluids, 9, 31-43

Koch T., H. G., Zettl T. und Sommer K. (1996). Mischzeitbestimmung an einem horizontalen Einwellenmischer. Schüttgut 2, 67-72

Landwehr F. (2005). Entwicklung eines Lichtleiterverfahrens zur Charakterisierung von Mehrphasenströmungen. Dissertation Universität Dortmund

Lee H.-S., J.-Y.L. and Yu M.-Y. (2005). Influence of inorganic pigments on the fluidity of cement mortars, Cement and Concrete Research 35, 703-710

Merz A. (1973). Untersuchung zur Axialvermischung in einem kontinuierlich betriebenen Drehrohr mit Isotopenmarkierung. Dissertation Universität (TH) Karlsruhe

Metcalfe, G., Shinbrot, T., McCarthy, J. J. and Ottino, J. M., (1995). Avalanche mixing of granular solids. 374, 39-41

Muzzio, F. J., Robinson, P., Wightman, C. and Brone, D., (1997). Sampling practices in powder blending. International Journal of Pharmaceutics, 155, 153-178

Muzzio, F. J., Llusa, M., Goodridge, C. L., Duong, N.-H. and Shen, E., (2008). Evaluating the mixing performance of a ribbon blender. Powder Technology, 186, 247-254

Müller W. (1966). Untersuchung über Mischzeit, Mischgüte und Arbeitsbedarf in Mischtrommeln mit rotierenden Mischelementen. Dissertation Universität (TH) Karlsruhe

Pahl M. H., Hoffmann. T. (1992). Qualitätssicherung in der Mischtechnik, Quality control in mixing technology. AT Aufbereitungstechnik/Mineral Processing 33, 605-612

Pahl M., Sommer K. et al. (1993). Mischen von Kunststoff- und Kautschukprodukten, VDI Verlag Kunststofftechnik, ISBN 3-18-234183-9

Puyvelde D. R. Van, B. R. Y., M. A. Wilson, S. J. Schmidt (1999). Experimental determination of transverse mixing kinetics in a rolling drum by image analysis. Powder Technology 106, 183-191

Puyvelde D. R. V. (2006). Simulating the mixing and segregation of solids in the transverse section of a rotating kiln. Powder Technology 164, 1-12

Raasch J., Elsässer B. (1995). Comparison of the Mixing Quality of a Continuous Mixer and a Batch Mixer. Bulk Solids Handling 16, 245-251

Realpe, A. and Velázquez, C., (2003). Image processing and analysis for determination of concentrations of powder mixtures. Powder Technology, 134, 193-200

Rose H. E (1959). A suggested equation relating to the mixing of powders and its application to the study of performance of certain types of machine, Trans. Instn. Chem. Engrs. 37, 139-156

Stalder B. (1993). Ermittlung der Mischgüte beim Pulvermischen. Dissertation ETH Zürich

Schulze D. (1995). Zur Fließfähigkeit von Schüttgütern- Definition und Messverfahren. Chemie-Ingenieur-Technik, 67, 60-68

Schulze D. (1998). Die Charakterisierung von Schüttgütern für Siloauslegung und Fließfähigkeitsuntersuchungen, The Characterization of bulk solids for silo design and folwability test. AT Aufbereitungstechnik/Mineral Processing 39, 47-57

Sommer K. (1979). Powder mixing mechanism, Jour. of Powder & Bulk solids Technology 3, 2-9

Sommer K. (1982). Wie vergleicht man die Mischfähigkeit von Feststoffmischern?, How to compare the mixing aptitude of mixers for solid materials?, AT Aufbereitungstechnik/Mineral Processing 23, 266-269

Stange K. (1963). Die Mischgüte einer Zufallsmischung aus drei und mehr Komponenten. Chemie-Ingenieur-Technik 35, 580-582

Wang R., Fan L.T. (1976). Axial mixing of grains in a motionless sulzer (Koch)mixer, Ing. Eng. Progr. 51, 27-36

Wightman Carolyn, F. J. M., Wilder Joseph (1996). A quantitative image analysis method for characterizing mixtures of granular materials. Powder Technology 89, 165-176

Weinekötter R. (1993). Kontinuierliches Mischen feiner Feststoffe. Dissertation ETH Zürich

Table Captions

Table 1 Pigments for replacing the cement

Table 2 Powder Properties

Table 3 Dispersion coefficients in relation to differing zero mixture charges, (a) side view of zero mixtures, (b) top view of zero mixtures

Figures Captions

Fig. 1. View of the mixing chamber of the twin-shaft-paddle laboratory mixer with spiral mixing tool

Fig. 2. Side view of the perpendicularly positioned video camera

Fig. 3. Determination of flow site according to Jenike

Fig. 4. Analysis algorithm for the determination of the mixing efficiency and the concentration efficiency

Fig. 5. Determination of the concentration field on the mixer surface (a) binary digital image, (b) concentration field without reduction, (c) concentration field with reduction

Fig. 6. Initial condition of the three moisten particle fractions without zero mixture from tracer

Fig. 7. Concentration efficiency about the mixing time in the twin-shaft-paddle mixer, starting with the zero mixture

Fig. 8. Concentration efficiency about the dimensionless length in the twin-shaft-paddle mixer, starting with the zero mixture

Fig. 9. Mixing efficiency of the twin-shaft-paddle mixer, starting with the zero mixture, Samples N_S=120, m_S=2.8g, D=232.6cm^2/s

Fig. 10. Mixing efficiency of the twin-shaft-paddle mixer, starting with the zero mixture, Samples N_S=120, m_S=2.8g, D=189.7cm^2/s

Fig. 11. Mixing efficiency of the twin-shaft-paddle mixer, starting with the zero mixture, Samples N_S=120, m_S=2.8 g, D=245.6 cm^2/s

Figure 1

Figure 2

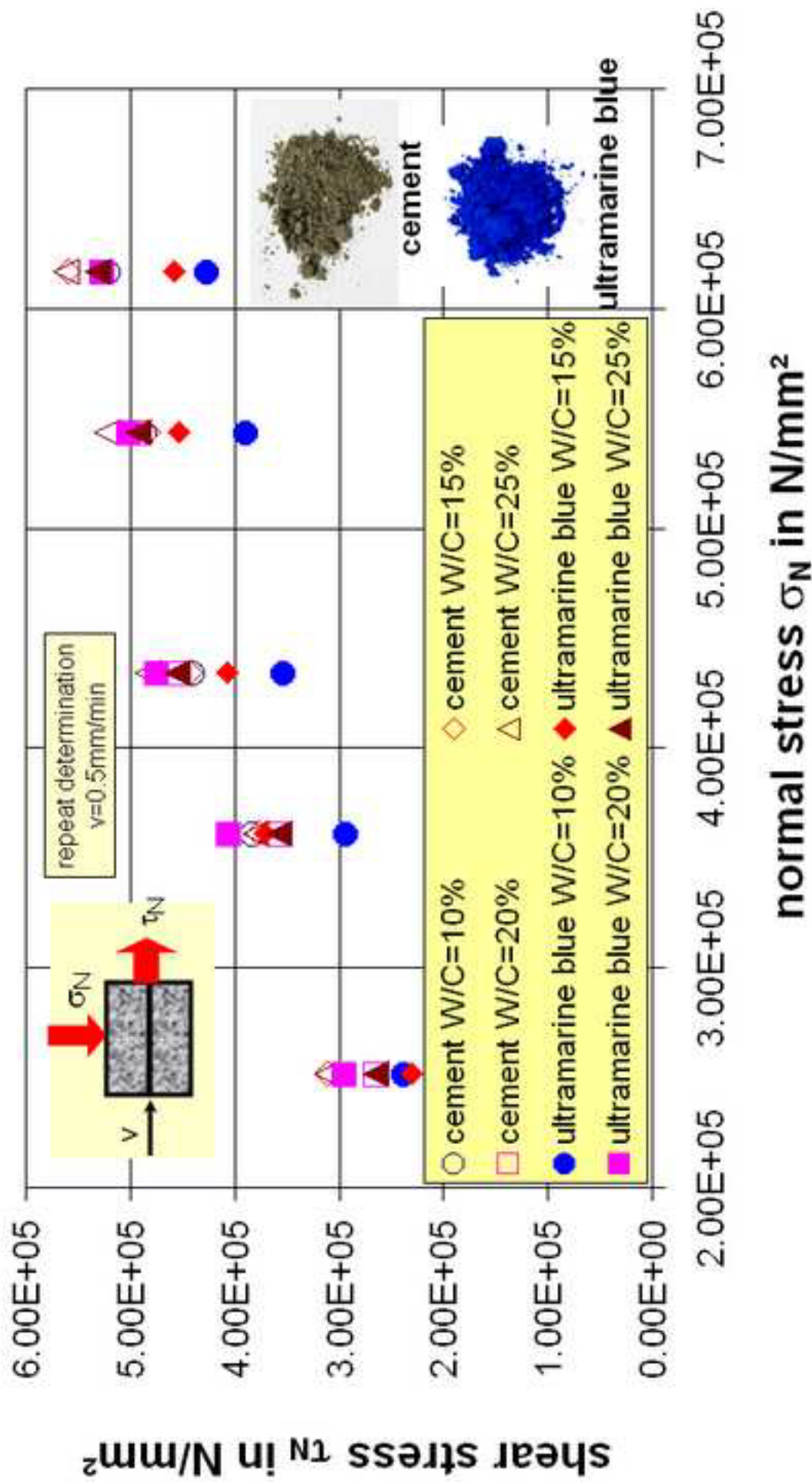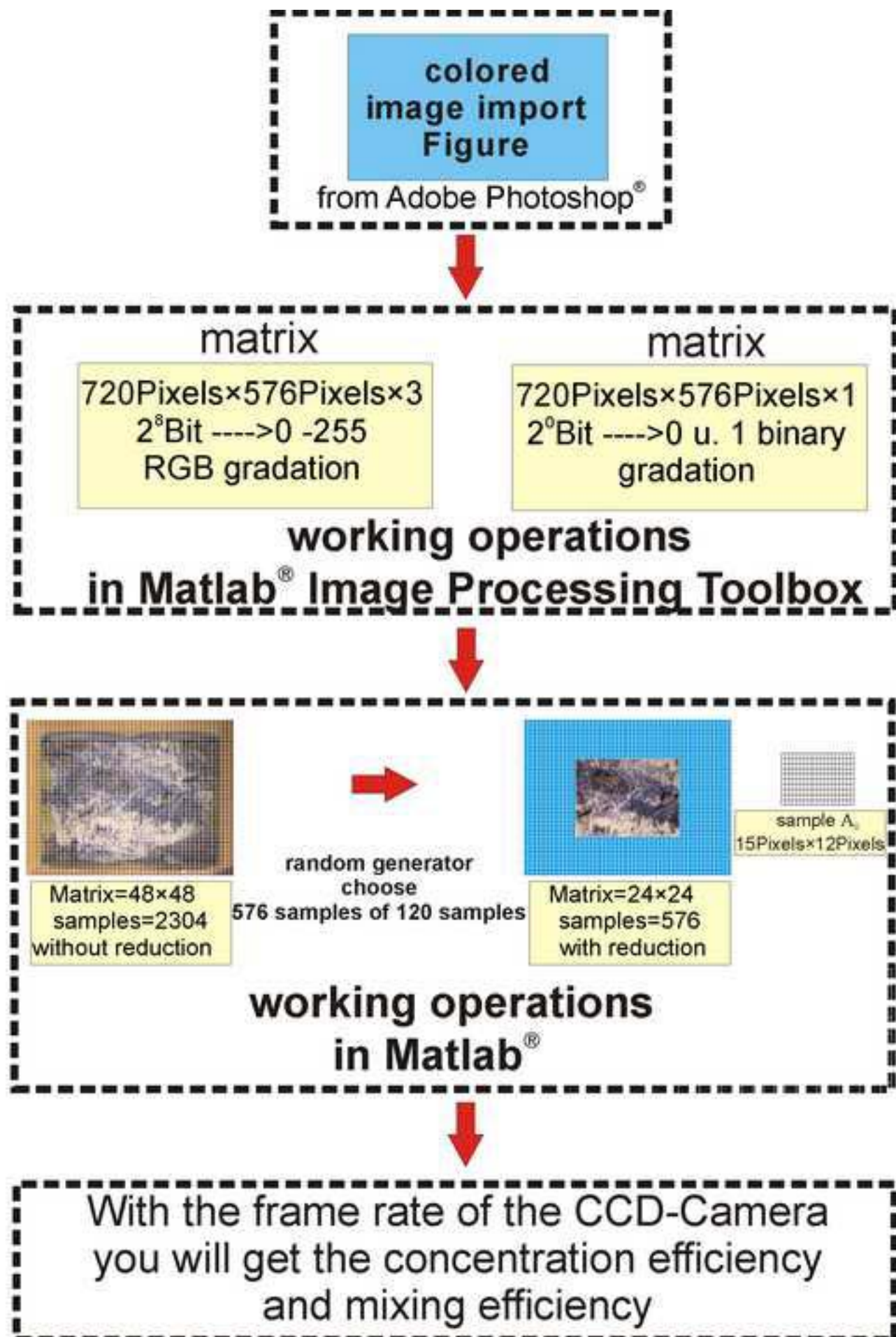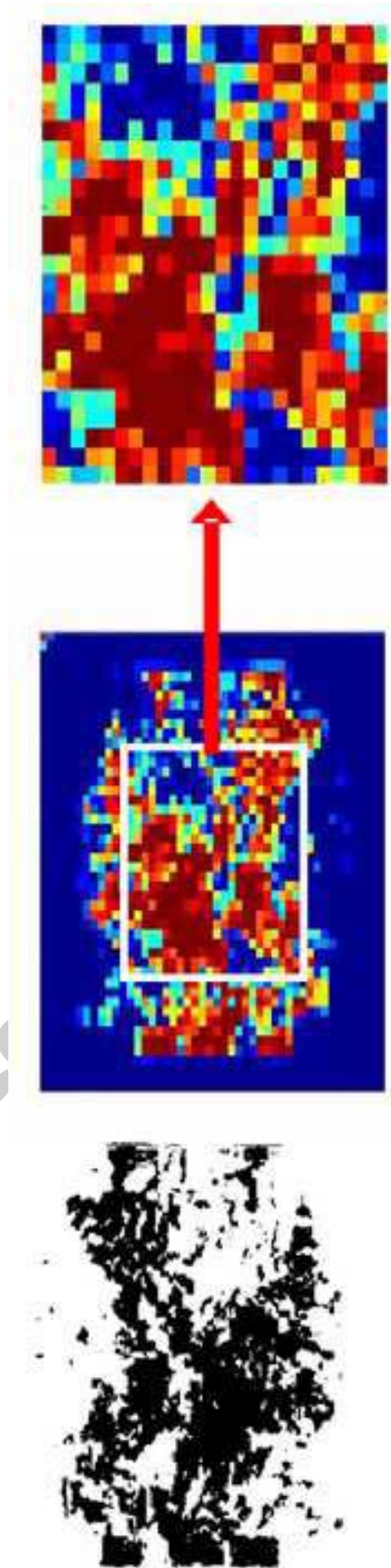**Figure 3**

Figure 4
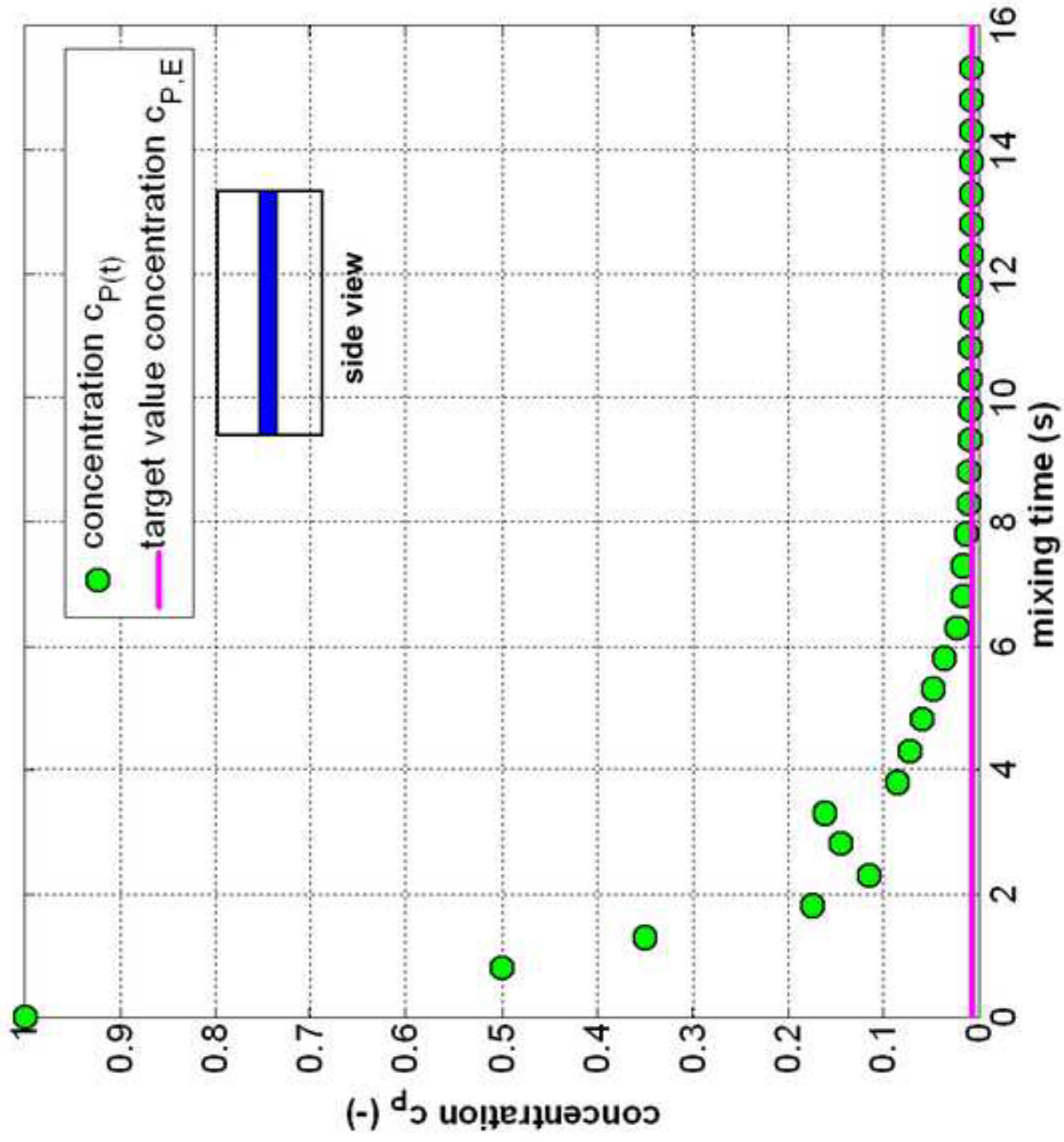
Figure 5
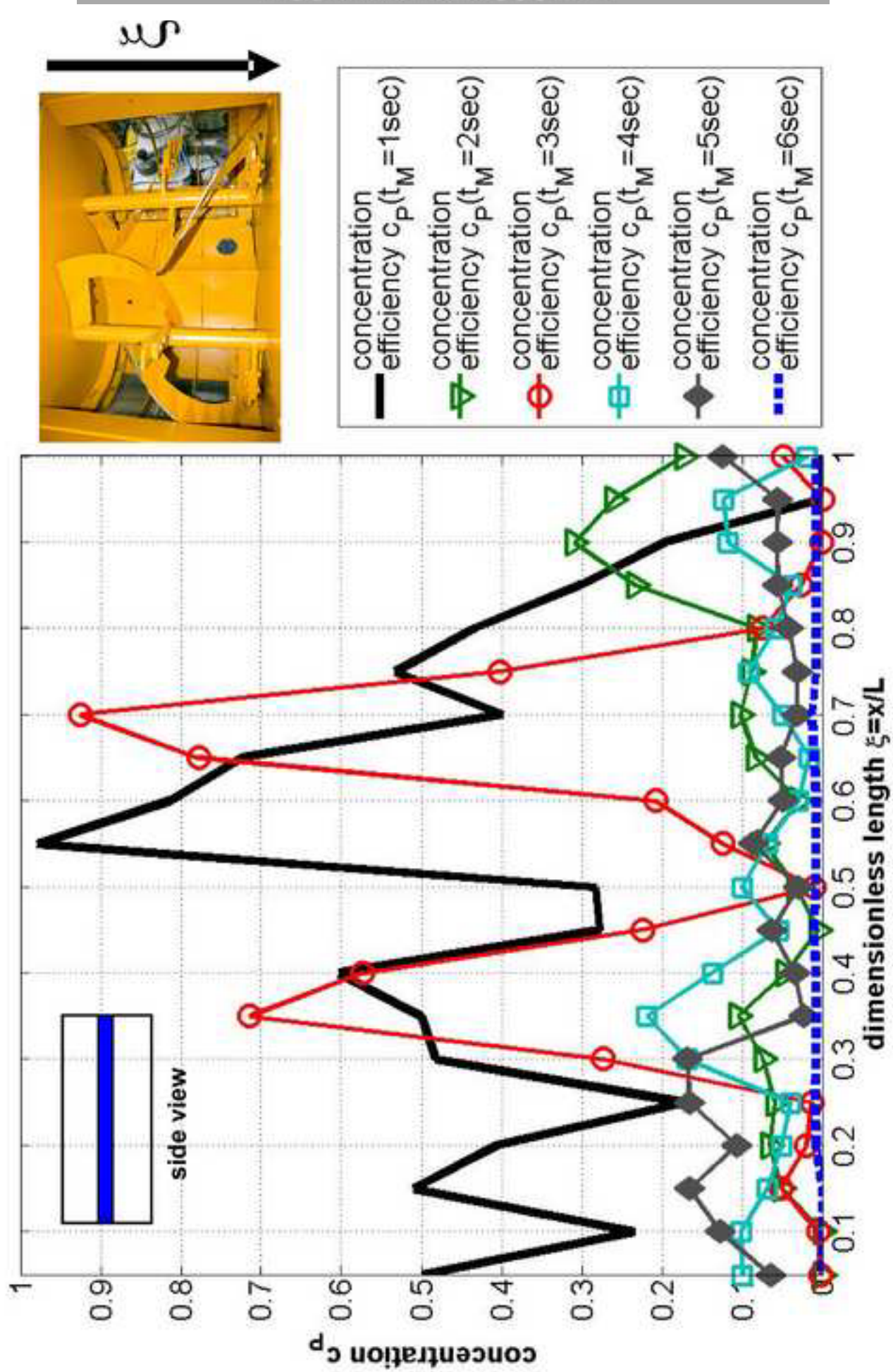
Figure 6
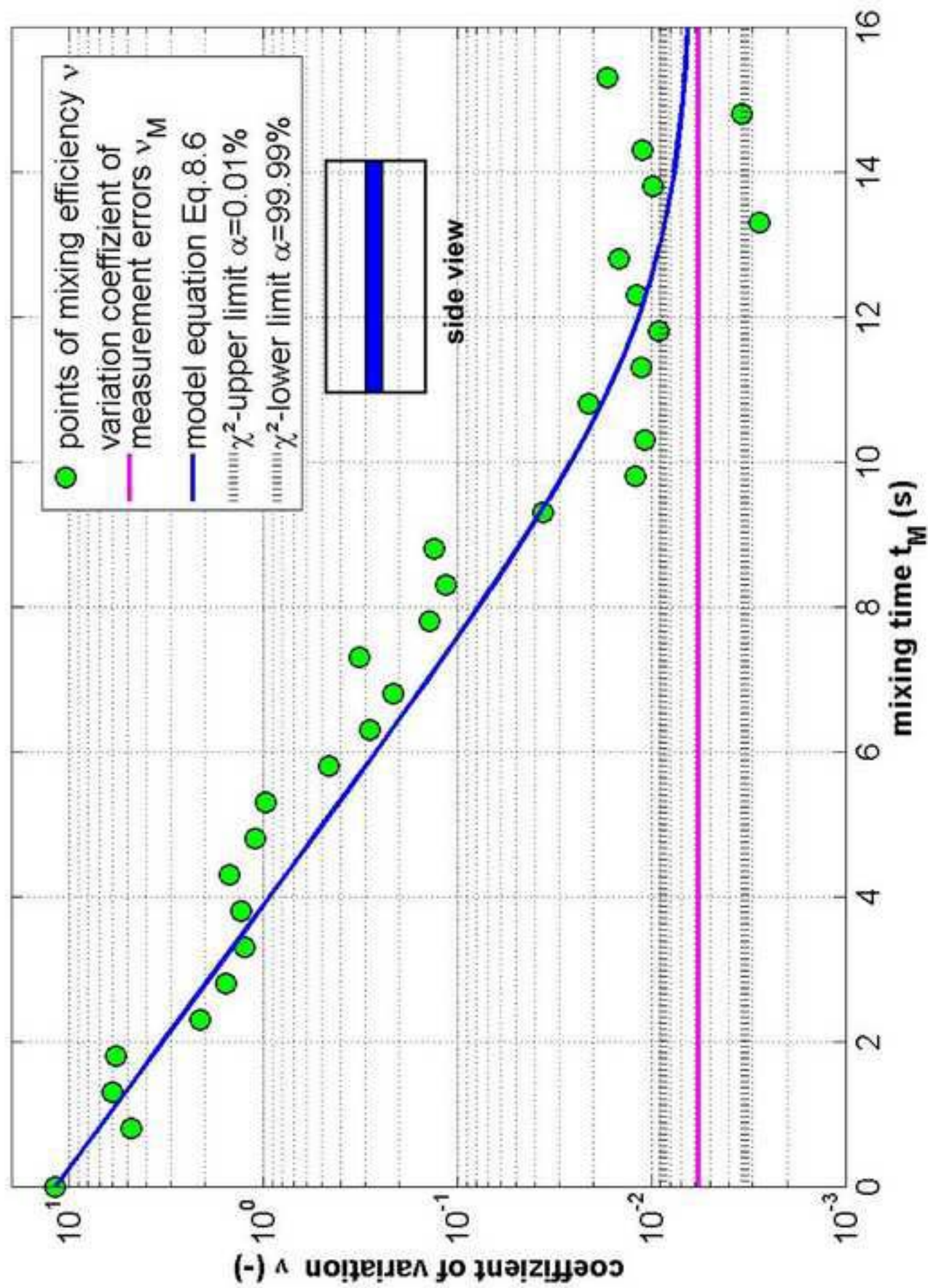
Figure 7

Figure 8

Figure 9

Figure 10

Figure 11